Contributions to Mineralogy and Petrology (2021) 176:42
https://doi.org/10.1007/s00410-021-01797-2

ORIGINAL PAPER

Thermal diffusivity and thermal conductivity of alkali feldspar at 0.8–3 GPa and 300–873 K

Zili Xiong[1,2] · Baohua Zhang[1,3] · Jianhua Ge[1,2] · Shuangmeng Zhai[1] · Xinzhuan Guo[1]

Received: 3 December 2020 / Accepted: 28 April 2021 / Published online: 11 May 2021

Abstract

The heat transport properties of feldspar, one of the major minerals of the crust, are important for constraining the thermal state of the Earth's crust. The thermal diffusivity (D) and thermal conductivity (κ) of two natural alkali feldspars, namely, perthite and albite (Ab), were simultaneously measured at high temperatures (300–873 K) and high pressures (0.8–3 GPa) using a transient plane-source method. The present results show that the D and κ of these alkali feldspars decreased with the increase in temperature, whereas the κ of perthite remained almost constant at above 450 K. The D and κ of these samples decreased by 24–35% and 8–21% when the temperature increased from 300 to 873 K, respectively, suggesting that phonon conduction may be the dominant mechanism. The D and κ of these samples also exhibited a positive pressure dependence as indicated by their positive pressure coefficients: 0.052–0.098 $mm^2s^{-1}GPa^{-1}$ for D and 0.189–0.325 $Wm^{-1}K^{-1}GPa^{-1}$ for κ. Combining previous data with the results of this study, the D and κ of an intermediate albite-orthoclase solid solution can be reasonably estimated by an empirical model. Furthermore, the average κ of the crust was recalculated to accurately constrain the thermal thickness and temperature of the lithosphere. The present estimate suggests that partial melting can occur at shallow depths of the middle and lower crust, which may provide a new understanding of the low-velocity and high-conductivity anomalies revealed by geophysical observations in the crust.

Keywords Thermal diffusivity · Thermal conductivity · Alkali feldspar · Crust

Introduction

Temperature gradients within the Earth are the driving force for numerous dynamic processes on various scales. To understand and model heat transfer in the Earth's interior, such as mantle convection (Yanagawa et al. 2005) and melting of the crust and subducting plate (Zheng and Chen 2016), data on heat transport properties of the Earth's constituent phases are required (e.g., Anderson 1999; Hofmeister 1999). Feldspars are the most abundant minerals of the Earth's crust, they comprise 60 vol.% of the Earth's crust (Smith and Brown 1988), occurring widely in sedimentary, igneous, and metamorphic rocks. Therefore, the measurement of thermal transport properties of feldspars is crucial for understanding heat transfer in crustal rocks and modeling geothermal gradient.

Feldspars mainly include three end members: $NaAlSi_3O_8$ [albite (Ab)], $KAlSi_3O_8$ [orthoclase (Or)], and $CaAl_2Si_2O_8$ [anorthite (An)]. At elevated temperatures, complete solid solutions form between Ab and Or components and between Ab and An components, which are known as alkali feldspars and plagioclase. To date, several studies have reported the thermal properties of feldspar. Kanamori et al. (1968) first measured the thermal diffusivity (D) of alkali feldspar using the Ångström method. They observed that D increased with the increase in temperature. Höfer and Schilling (2002) measured D of Or and

Communicated by Hans Keppler.

✉ Baohua Zhang
zhangbaohua@zju.edu.cn

✉ Xinzhuan Guo
gxzhuan@mail.gyig.ac.cn

[1] Key Laboratory for High-Temperature and High-Pressure Study of the Earth's Interior, Institute of Geochemistry, Chinese Academy of Sciences, Guiyang 550081, China

[2] University of Chinese Academy of Sciences, Beijing 100049, China

[3] Key Laboratory of Geoscience Big Data and Deep Resource of Zhejiang Province, School of Earth Sciences, Zhejiang University, Hangzhou 310027, China

sanidine under 1 atm pressure and elevated temperatures by a transient method, and a small temperature dependence of up to 623 K was observed for both feldspars. At elevated temperatures above 623 K, the D of sanidine showed a stronger dependence expressed as $D \propto T^3$. The contribution of radiative heat-transfer led to more than twice higher D in sanidine than in Or at 1073 K. Pertermann et al. (2008) and Hofmeister et al. (2009) measured the D of single-crystal Ab, sanidine, near-endmember feldspar glasses, and melts using the laser-flash analysis (LFA) under 1 atm pressure and high temperature. They observed that the D of glass decreased with the increase in temperature, and it decreased more rapidly upon crossing the glass transition point. Consequently, the D and inferred thermal conductivity (κ) for the melt are consistently below those of bulk crystal or glass. Branlund and Hofmeister (2012) investigated the D of six natural plagioclase crystals as a function of temperature and composition ($An_{5\text{-}95}$) at 1 atm pressure. Their data showed that the D of plagioclase solid solution increased with the Ab content, indicating a composition effect on thermal diffusivity. The substitution between Na and Ca in plagioclase caused Al-Si disorder to reduce the thermal diffusivity.

It is worth noting that in all of previous studies (Kanamori et al. 1968; Höfer and Schilling 2002; Pertermann et al. 2008; Hofmeister et al. 2009; Branlund and Hofmeister 2012), only the D of feldspar was measured at elevated temperatures, and no direct measurements have been performed on the κ of feldspar. The available κ for feldspar is roughly estimated from $\kappa = C_P D \rho$, where ρ is the density, and C_P is the heat capacity. This approach may cause large uncertainties because of the different starting materials used in the measurements of thermal diffusivity and heat capacity. The possible effect of chemical composition, grain size, porosity, microstructure, and lattice distortion of the starting materials on heat capacity have not been well evaluated. Pressure imposes an important effect on D and κ and eventually affects heat capacity (Wang et al. 2014; Fu et al. 2019; Zhang et al. 2019a; Xiong and Zhang 2019). By measuring D and κ simultaneously, the transient plane-source method can overcome the disadvantage mentioned above. Given that all previous experiments on D of feldspar have been conducted under 1 atm pressure, the influence of pressure on thermal properties of feldspar is still unknown. The pressure effect should also be determined to better constrain the thermal thickness of the lithosphere.

In this study, we performed in-situ measurements of D and κ of two natural alkali feldspars (perthite and Ab) simultaneously under high pressure (0.8–3 GPa) and temperature (300–873 K). The effects of temperature, pressure, chemical composition, sample thickness, and heating or cooling history on the thermal transport properties of samples are discussed. Furthermore, the κ of the average crust was calculated to re-evaluate the temperature and thickness of the lithosphere.

Experimental methods

Sample preparation

Two natural alkali feldspar samples (perthite and Ab) were collected from Hebei Province, China. Thin-section observations (Fig. 1) showed that the perthite sample contained ~ 30 vol.% Ab as exsolution lamellae ($Na_{0.5}Ca_{0.1}Al_{1.1}Si_{2.9}O_8$ in composition) and ~ 70 vol.% potassium-rich microcline as the host mineral with a distinct grid twin (Fig. 1a). Polysynthetic and Kana composite twins were observed in the Ab sample ($Na_{0.6}Ca_{0.1}Al_{1.1}Si_{2.9}O_8$ in composition, Fig. 1b). Table 1 lists the chemical compositions of both samples analyzed by an electron probe microanalyzer.

Disks with 6 mm diameter and without visible cracks were cored and cut into pieces with ~ 1.1 mm thickness. To

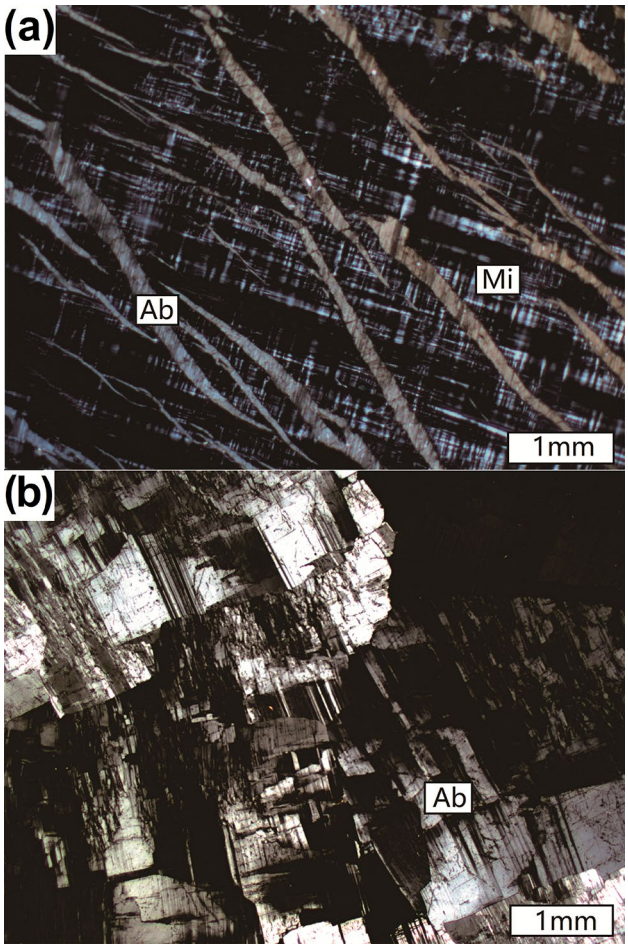

Fig. 1 Microstructural images of perthite (**a**) and albite (**b**) under crossed polarized light. Ab = Albite, Mi = Microcline

Table 1 Chemical composition of the perthite and albite

Oxide (wt%)	Perthite		Albite $Ab_{82}An_{17}Or_1$ ($N=7$)
	Or_{100} ($N=8$)	$Ab_{79}An_{19}Or_2$ ($N=8$)	
SiO_2	63.16 (1.24)	66.85 (1.15)	66.22 (1.45)
Al_2O_3	17.79 (0.76)	22.51 (0.87)	22.13 (0.33)
FeO	0.01 (0.01)	0.05 (0.01)	0.12 (0.01)
MnO			0.12 (0.01)
MgO			0.52 (0.03)
CaO	0.01 (0.01)	2.92 (0.35)	2.64 (0.21)
Na_2O	0.78 (0.17)	6.73 (0.61)	7.12 (0.37)
K_2O	17.47 (1.68)	0.25 (0.01)	0.16 (0.01)
Total	99.27	99.31	99.03

N denotes numbers of analysis and numbers in parentheses are 1σ deviation from the mean

Or orthoclase, *Ab* albite, *An* anorthite

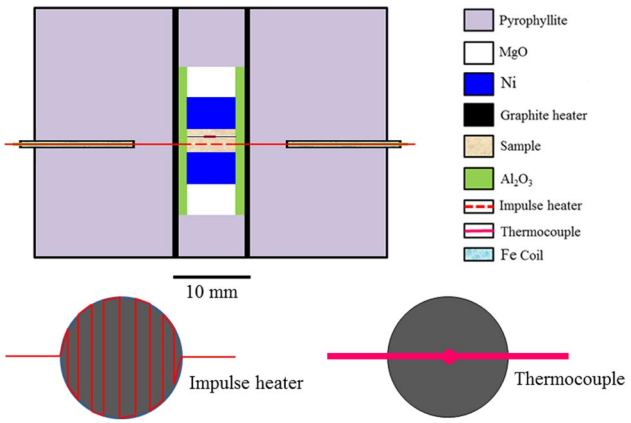

Fig. 2 Schematic cross section of sample assembly for thermal properties measurement

minimize the contact resistance during thermal properties measurements, we first polished both surfaces of the specimens with sandpaper and then with a 0.25 μm diamond powder. The samples were cleaned in acetone and ethanol using an ultrasonic cleaner and kept in a vacuum oven at 473 K for 24 h to remove any possible absorbed water before assembly.

Measurement of *D* and *κ*

In-situ measurements of thermal properties (D and κ) were carried out at 0.8–3 GPa and 300–873 K using the transient plane-source method (Dzhavadov 1975; Osako et al. 2004, 2010), in a DIA-type multi-anvil apparatus (YJ-3000t) at the Institute of Geochemistry, Chinese Academy of Sciences. Figure 2 shows the cell design for thermal property measurement, which is the same as that in our previous work (Fu et al. 2019; Zhang et al. 2019a; Ge et al. 2021). A pyrophyllite cube and a graphite sleeve were used as the pressure-transmitting medium and heater, respectively. Samples were isolated from the graphite heater using an Al_2O_3 sleeve, which also served as a heat insulator to effectively restrict lateral heat flow. Three thin disks with nearly identical double-polished specimens were piled face to face at the center of the sample chamber. A thin, flat K-type (NiCr–NiAl) thermocouple was inserted between the sample disks to monitor temperature. A planar nickel-chromium heater with the same diameter as the sample (Fig. 2) was placed at the other interface of the sample disks to induce impulse heating. Two nickel blocks in direct contact with the sample were used as heat sinks to ensure a constant-temperature boundary condition. Pressure was calibrated from the melting curve of NaCl at high temperature and the phase transformation of bismuth (2.54 GPa) at ambient temperature. The precisions of pressure estimation and temperature measurement were approximately 0.5 GPa and 1 K, respectively.

During measurement, the sample was heated up to 873 K at each desired pressure and then cooled to room temperature in steps of 50 or 100 K. At least three heating–cooling cycles were conducted to assess the reproducibility. The thermal disturbance caused by impulse heating was monitored by the thermocouple (Fig. 3). Temperature variation ΔT at the position of the thermocouple can be expressed as follows (Dzhavadov 1975; Osako et al. 2004):

$$\Delta T = A\sum_{n=1}^{\infty}\frac{1}{n^2}\sin\frac{n\pi}{3}\sin\frac{n\pi x}{d}\exp(-n^2Bt)\left[\exp(n^2B\tau)-1\right] : (t>\tau) \quad (1)$$

where x is the distance (m) between the impulse heater and the thermocouple, d is the total height (m) of three sample disks, t is the time (s) from the onset of heating, and τ is the duration (s) of impulse heating. The quantities A and B are defined as below:

$$A = \frac{2Qd}{\pi^2\kappa S}, \quad B = \frac{\pi^2 D}{d^2} \quad (2)$$

where S is the area (m^2) of the impulse heater, Q is the power (W) of impulse heating, D and κ are the thermal diffusivity (mm^2s^{-1}) and thermal conductivity ($Wm^{-1}K^{-1}$), respectively. Previous studies (Dzhavadov 1975; Osako et al. 2004) demonstrated that Eq. (1) was valid at a constant temperature when both ends of the sample were set as boundary conditions. Consequently, the parameters A and B can be determined through the least-square fitting of the converted temperature–time curves using Eq. (1) by changing n up to 15 (Fig. 3). Once A and B are known, D and κ can be calculated from Eq. (2) when combined with other parameters. As discussed in previous studies (e.g., Osako et al. 2004; Wang et al. 2014; Fu et al. 2019; Zhang et al. 2019a; Ge et al. 2021), the accuracy of D and κ mainly derives from the

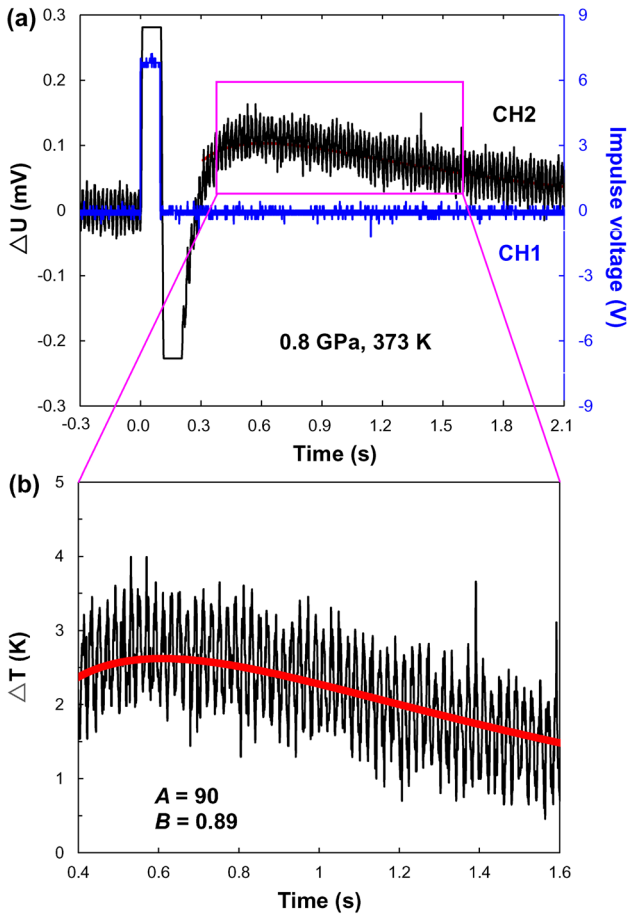

Fig. 3 **a** A record of oscilloscope display for perthite sample (1.1 mm) under 0.8 GPa and 373 K in the present study. CH1 and CH2 are used to monitor the pulse heater voltage and thermocouple output, respectively. **b** A typical example shows that the corresponding temperature time curve (converted from the digitized data of the voltage time curve output by the thermocouple as shown by the dotted rectangle in (**a**) is used for data fitting to determine parameters *A* and *B* in Eq. (2)

uncertainty of sample thickness (*d*), area of heater (*S*), pulse heating power (*Q*), temperature, and the least-square fitting of parameters *A* and *B* in Eq. (2). The dimension of samples during measurement was corrected from the equation of state of Ab and microcline (Benusa et al. 2005; Nestola et al. 2008). The area change of the pulse heater was calculated in accordance with the method proposed by Wang et al (2014). The temperature perturbation across the sample disk due to pulse heating was about 3 K by applying a pulse power of 10 W. Thus, the influence of temperature heterogeneity on the measured results was negligible in the present assembly. As a result, the total experimental errors in Eq. (2) originating from the above-mentioned factors were estimated to be less than 5% in this study (Table 2).

Experimental results

D and *κ* of perthite

Figure 4a, b show the temperature dependence of *D* and *κ* of perthite at 0.8–3 GPa, respectively. Table 2 summarizes all data of *D* and *κ* under high *P*–*T* conditions. At each pressure, a decreasing and concave-up trend between *D* and *κ* and temperature can be fitted by the following empirical relations (Hofmeister 1999; Hofmeister et al. 2014):

$$D(T) = a_1 + a_2 \times T^{-1} + a_3 \times T^{-2} + a_4 \times T^{-3} \quad (3)$$

$$\kappa(T) = b_1 + b_2 \times T^{-1} + b_3 \times T^{-2} + b_4 \times T^{-3} \quad (4)$$

where *T* is the absolute temperature, and the fitting results for coefficients a_1, a_2, a_3, a_4, b_1, b_2, b_3, and b_4 are given in Table 3. In the whole experimental temperature range, the *D* of perthite gradually decreased with the increase in temperature (Fig. 4a). At 0.8 GPa, the *D* values reduced from 1.2 mm^2s^{-1} at 300 K to 0.8 mm^2s^{-1} at 825 K, and a similar drop (~ 34%) was observed at other pressures. However, the temperature dependence weakened when it was higher than ~ 450 K for all pressures (Fig. 4b). These observations suggest that the feldspar sample was not heated by protons given that the probability of the absorption and emission process was extremely low. Thus, phonon conduction was the main mechanism. Moreover, the *D* and *κ* of the perthite systematically increased with the increase in pressure at each constant temperature (Fig. 4c, d). The variation of *D* and *κ* with pressure can be linearly fitted to the following empirical forms (Hofmeister 2007; Hofmeister et al. 2014):

$$D(P) = D_0 + c_1 \times P \quad (5)$$

$$\kappa(P) = \kappa_0 + d_1 \times P \quad (6)$$

where the fitting parameters D_0, c_1, κ_0, and d_1 are summarized in Table 3. The calculated pressure coefficients (c_1 and d_1) of *D* and *κ* for perthite were in the range of 0.047–0.084 $mm^2s^{-1}GPa^{-1}$ and 0.191–0.261 $Wm^{-1}K^{-1}GPa^{-1}$, respectively. The pressure coefficients (c_1 and d_1) of *D* and *κ* decreased with the increase in temperature.

Figure 5a, b show the *D* and *κ*, respectively, of perthite based on the data collected during heating and cooling of the sample at 2 GPa. A high reproducibility during heating and cooling cycles was achieved using the transient plane-source method in this study. On the other hand, a comparative experiment with a thicker perthite sample (~1.45 mm) was performed under the same *P*–*T* conditions to investigate the effect of sample thickness on the resulting thermal properties. Tables 2, 3 and Supplementary Tables 1–2 summarize the raw data and fitting parameters, respectively. Although

Table 2 Thermal diffusivity (D) and thermal conductivity (κ) of perthite and albite as a function of temperature at given pressure

T (K)	0.8 GPa D (mm^2s^{-1})	0.8 GPa κ ($Wm^{-1}K^{-1}$)	1.5 GPa D (mm^2s^{-1})	1.5 GPa κ ($Wm^{-1}K^{-1}$)	2.0 GPa D (mm^2s^{-1})	2.0 GPa κ ($Wm^{-1}K^{-1}$)	2.5 GPa D (mm^2s^{-1})	2.5 GPa κ ($Wm^{-1}K^{-1}$)	3.0 GPa D (mm^2s^{-1})	3.0 GPa κ ($Wm^{-1}K^{-1}$)
Perthite										
290	1.209 (7)	1.620 (7)	1.261 (9)	1.778 (8)	1.292 (54)	1.904 (13)	1.344 (32)	2.016 (9)	1.397 (13)	2.209 (10)
323	1.055 (8)	1.557 (8)	1.118 (8)	1.688 (8)	1.149 (9)	1.830 (9)	1.202 (8)	1.959 (7)	1.233 (7)	2.104 (9)
373	0.978 (10)	1.522 (12)	1.020 (20)	1.637 (11)	1.062 (10)	1.789 (12)	1.104 (9)	1.917 (10)	1.146 (11)	2.028 (12)
423	0.945 (16)	1.521 (17)	0.976 (17)	1.625 (17)	1.029 (19)	1.770 (18)	1.060 (10)	1.883 (17)	1.091 (11)	1.983 (20)
473	0.901 (20)	1.516 (23)	0.932 (21)	1.613 (22)	0.974 (20)	1.755 (26)	1.006 (21)	1.869 (21)	1.047 (17)	1.973 (24)
523	0.857 (22)	1.508 (28)	0.899 (19)	1.609 (28)	0.941 (13)	1.742 (49)	0.973 (19)	1.853 (26)	1.004 (15)	1.958 (28)
573	0.846 (8)	1.507 (27)	0.877 (24)	1.582 (26)	0.908 (20)	1.738 (46)	0.940 (11)	1.851 (31)	0.971 (19)	1.937 (31)
623	0.835 (20)	1.505 (33)	0.866 (25)	1.588 (27)	0.897 (11)	1.710 (42)	0.929(19)	1.843 (30)	0.949 (26)	1.919 (51)
673	0.824 (19)	1.486 (33)	0.855 (18)	1.576 (32)	0.876 (22)	1.728 (39)	0.907 (19)	1.826 (33)	0.938 (17)	1.915 (29)
723	0.813 (18)	1.494 (31)	0.844 (23)	1.597 (32)	0.865 (22)	1.725 (41)	0.896 (16)	1.813 (34)	0.916 (15)	1.930 (35)
773	0.802 (18)	1.493 (34)	0.833 (16)	1.579 (33)	0.854 (21)	1.722 (38)	0.885 (14)	1.809 (32)	0.906 (13)	1.908 (31)
823	0.802 (19)	1.486 (33)	0.833 (19)	1.584 (31)	0.854 (21)	1.719 (41)	0.885 (16)	1.813 (31)	0.906 (12)	1.890 (32)
Albite										
290	1.112 (9)	1.580 (9)	1.176(9)	1.794 (21)	1.231 (8)	1.986 (8)	1.276 (8)	2.141 (9)	1.322 (8)	2.284 (9)
323	1.076 (9)	1.511 (10)	1.130(9)	1.685 (15)	1.176 (6)	1.917 (8)	1.231 (8)	2.048 (12)	1.267 (8)	2.150 (15)
373	1.030 (8)	1.461 (10)	1.094(8)	1.629 (17)	1.130 (5)	1.864 (7)	1.185 (7)	1.966 (8)	1.212 (7)	2.084 (11)
423	1.003 (9)	1.425 (10)	1.048(7)	1.593 (17)	1.112 (6)	1.814 (9)	1.149 (7)	1.917 (9)	1.176 (8)	2.049 (11)
473	0.948 (7)	1.411 (13)	1.021(9)	1.567 (19)	1.076 (7)	1.772 (8)	1.130 (8)	1.894 (12)	1.158 (17)	1.991 (13)
523	0.921 (9)	1.401 (17)	0.984(9)	1.520 (22)	1.048 (7)	1.706 (10)	1.103 (8)	1.827 (11)	1.139 (9)	1.942 (12)
573	0.893 (9)	1.383 (17)	0.957(18)	1.520 (29)	1.003 (9)	1.697 (12)	1.066 (9)	1.779 (13)	1.103 (7)	1.896 (15)
623	0.848 (17)	1.389 (25)	0.921(17)	1.510 (28)	0.984 (8)	1.671 (13)	1.039 (9)	1.772 (14)	1.066 (9)	1.862 (16)
673	0.838 (9)	1.394 (20)	0.902(16)	1.491 (30)	0.957 (9)	1.667 (13)	1.003 (17)	1.750 (15)	1.048 (9)	1.841 (16)
723	0.829 (18)	1.391 (26)	0.884(18)	1.494 (31)	0.930 (8)	1.632 (12)	0.975 (8)	1.741 (20)	1.030 (8)	1.808 (18)
773	0.820 (18)	1.383 (28)	0.875(9)	1.496 (33)	0.930 (9)	1.630 (10)	0.984 (8)	1.712 (16)	1.012 (10)	1.816 (18)
823	0.802 (18)	1.382 (32)	0.866(9)	1.482 (21)	0.921 (7)	1.615 (15)	0.966 (17)	1.724 (27)	1.012 (9)	1.808 (30)
873	0.793 (27)	1.371 (30)	0.857(18)	1.478 (34)	0.911 (9)	1.597 (16)	0.966 (17)	1.697 (31)	1.003 (26)	1.775 (23)

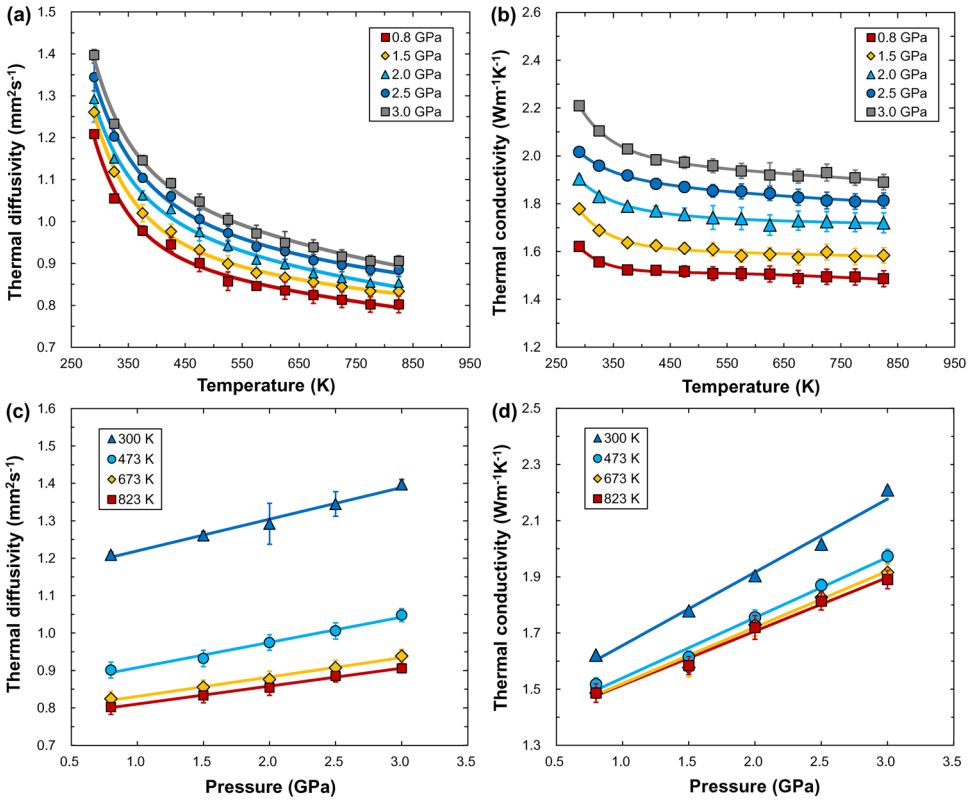

Fig. 4 Effect of temperature and pressure on thermal properties of perthite. Temperature dependence of D **(a)** and κ **(b)** at different pressure; pressure dependence of D **(c)** and κ **(d)** at temperature of 300, 473, 673, and 823 K

the largest difference was less than 0.1 mm^2s^{-1} for D and 0.1 $Wm^{-1}K^{-1}$ for κ (Fig. 5c, d), the values remain below experimental uncertainties. Therefore, sample thickness has negiligible influence on D and κ.

D and *κ* of Ab

Similar to the trends observed in perthite, D and κ for albite decrease with temperature and increase with pressure; the temperature effect becomes small at high temperatures (Fig. 6). Accordingly, the temperature and pressure dependences of D and κ of Ab investigated in the present experiments were fitted by Eqs. (3–4) and Eqs. (5–6), respectively, and the corresponding fitting parameters are summarized in Table 3. Remarkably, the pressure derivative for the D of Ab was almost constant (0.096–0.098 $mm^2s^{-1}GPa^{-1}$) at different temperatures, but the pressure derivative of κ (0.189–0.325 $Wm^{-1}K^{-1}GPa^{-1}$) gradually decreased with the increase in temperature. These pressure derivatives of D and κ for Ab were greater than those for perthite.

The pressure coefficients for perthite and Ab in this study are relatively high compared with those from earlier literature summarized by Hofmeister et al (2007). There are significant differences in the pressure coefficients obtained in different studies. The pressure coefficient for D was between 3 and 15% GPa^{-1}, whereas that for κ can exceed 30% GPa^{-1}. The pressure coefficients obtained in this study through experimental measurements deviate from the theoretical predictions of Hofmeister (2007). Hard minerals can be desirably predicted, whereas the prediction on soft ones is difficult due to severe deformation. Various errors arise from thermal contact, pore space, grain rotation, or initial compression of the micro-void phase. Therefore, the pressure coefficient of polycrystalline samples measured at low pressure is unlikely to represent the intrinsic behavior of hard materials.

Discussion

Comparison with previous data

With the increased temperature at 1 atm pressure, the D of alkali feldspar reported by Kanamori et al. (1968) first showed a slight decrease (< 450 K) and then a rapid increase (> 500 K). Similar to Kanamori et al.'s results, Höfer and Schilling (2002) reported that the D of single-crystal Or and sanidine increased with the increase in temperature and the estimated κ. The positive temperature dependences of D and κ ($\propto T^3$) observed by Kanamori et al. (1968) and Höfer and Schilling (2002) have been attributed to the contribution of radiative heat transport by photons. By contrast, Pertermann et al. (2008) measured the D of single-crystals sanidine ($Or_{92}Ab_8$) in three orientations up to 1200 K

Table 3 Coefficients of fitting parameters for thermal diffusivity (D) and thermal conductivity (κ) as functions of temperature and pressure

$D(T)=a_1+a_2\times T^{-1}+a_3\times T^{-2}+a_4\times T^{-3}$						$\kappa(T)=b_1+b_2\times T^{-1}+b_3\times T^{-2}+b_4\times T^{-3}$				
	a_1 (mm^2s^{-1})	a_2 ($mm^2s^{-1}K$)	a_3 ($mm^2K^2s^{-1}$)	a_4 ($mm^2K^3s^{-1}$)	R^2	b_1 ($Wm^{-1}K^{-1}$)	b_2 (Wm^{-1})	b_3 (WKm^{-1})	b_4 (WK^2m^{-1})	R^2
Perthite										
0.8 GPa	0.521 (148)	373 (214)	− 160,055 (98,228)	3.159 (1.42)E7	0.99	1.215 (70)	413 (102)	− 197,269 (46,772)	3.231 (676)E7	0.99
1.5 GPa	0.622 (80)	267 (116)	− 111,639 (53,161)	2.535 (768)E7	0.99	1.422 (119)	253 (173)	− 133,864 (79,122)	2.608 (1.14)E7	0.97
2.0 GPa	0.549 (137)	367 (199)	− 133,946 (90,974)	2.592 (1.31)E7	0.99	1.649 (97)	100 (141)	− 51,762 (64,473)	1.267 (932)E7	0.98
2.5 GPa	0.643 (107)	276 (155)	− 94,992 (71,055)	2.129 (1.02)E7	0.99	1.632 (65)	225 (95)	− 85,017 (43,569)	1.510 (629)E7	0.99
3.0 GPa	0.539 (140)	449 (203)	− 167,703 (93,156)	3.155 (1.34)E7	0.99	1.633 (100)	382 (155)	− 175,079 (71,061)	3.269 (1.02)E7	0.99
Albite										
0.8 GPa	0.691 (87)	8.4 (129)	88,593 (60,701)	− 1.62 (0.89)E7	0.99	1.342 (62)	58 (92)	− 36,599 (43,452)	1.151 (0.64)E7	0.99
1.5 GPa	0.663 (71)	145 (105)	23,860 (49,521)	− 6.75 (7.28)E6	0.99	1.392 (100)	99 (151)	− 34,179 (70,878)	1.118 (1.04)E7	0.98
2.0 GPa	0.614 (114)	303 (170)	− 50,632 (79,859)	4.053 (11.7)E6	0.99	1.478 (100)	56 (159)	54,909 (74,322)	− 8.393 (1.09)E7	0.99
2.5 GPa	0.647 (126)	328 (188)	− 60,619 (88,184)	5.180 (12.9)E6	0.99	1.529 (139)	132 (208)	13,731 (97,570)	− 3.201 (1.43)E7	0.99
3.0 GPa	0.646 (100)	411 (151)	− 111,679 (70,651)	1.424 (1.04)E7	0.99	1.417 (177)	402 (264)	− 96,676 (123,662)	1.500 (1.82)E7	0.98

$D(P)=D_0+c_1\times P$				$\kappa(P)=\kappa_0+d_1\times P$		
	D_0 (mm^2s^{-1})	c_1 ($mm^2s^{-1}GPa^{-1}$)	R^2	κ_0 ($Wm^{-1}K^{-1}$)	d_1 ($Wm^{-1}K^{-1}GPa^{-1}$)	R^2
Perthite						
300 K	1.135 (11)	0.084 (5)	0.98	1.394 (35)	0.261 (16)	0.98
473 K	0.840 (9)	0.067 (4)	0.98	1.324 (28)	0.215 (13)	0.98
673 K	0.779 (6)	0.052 (3)	0.98	1.319 (21)	0.200 (10)	0.99
823 K	0.762 (3)	0.047 (1)	0.99	1.323 (24)	0.191 (11)	0.98
Albite						
300 K	1.035 (3)	0.096 (1)	0.99	1.320 (17)	0.325 (8)	0.99
473 K	0.874 (11)	0.098 (5)	0.98	1.188 (39)	0.274 (18)	0.98
n673 K	0.761 (3)	0.096 (1)	0.99	1.212 (37)	0.212 (17)	0.97
n873 K	0.714 (7)	0.097 (3)	0.99	1.211 (16)	0.189 (8)	0.99

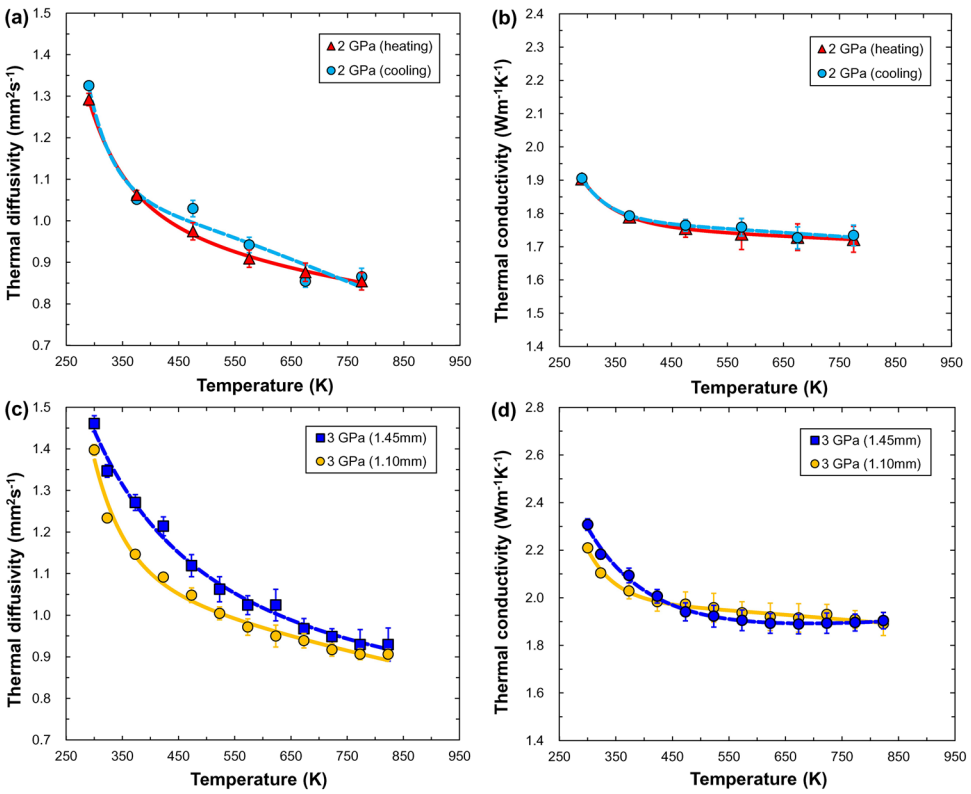

Fig. 5 Effects of thermal history (cooling and heating) and thickness on D and κ of perthite

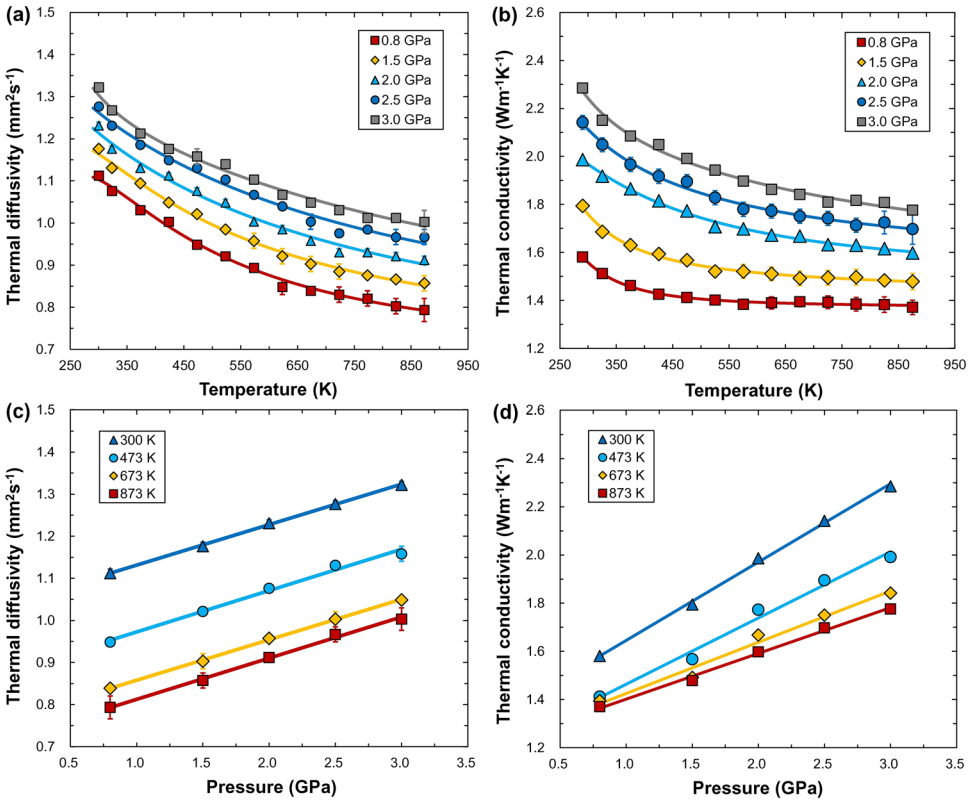

Fig. 6 Effect of temperature and pressure on thermal properties of albite. Temperature dependence of D **(a)** and κ **(b)** at different pressure; pressure dependence of D **(c)** and κ **(d)** at temperature of 300, 473, 673, and 873 K

using LFA. Their results indicated that the D of $Or_{92}Ab_8$ in three directions gradually decreased with the increase in temperature, which is consistent with our observations in this study (Fig. 7a). Pertermann et al. (2008) assumed that the experimental results from the works of Kanamori et al. (1968) and Höfer and Schilling (2002) may be problematic. At high temperature (> 450 K), the abnormally high D arose from the radiative heat-transfer mechanism caused by the diffused scattering by fluid inclusion and exsolution (Höfer and Schilling 2002). Radiative heat transfer is believed to occur at temperatures above 800 K. However, this process only occurs from at least 450 K, which is extremely low for radiative heat-transfer mechanism (Kanamori et al. 1968; Höfer and Schilling 2002). A single-contact method on the measurements of D was adopted by Kanamori et al. (1968) and Höfer and Schilling (2002). At 1 atm pressure, the direct contact of the thermocouple with samples led to excessive contact thermal resistance, which hindered the propagation of phonons and thus reduced the D. Hofmeister (2007) and Hofmeister et al. (2007) confirmed that the results from contact methods systematically deviate in opposite directions and to various degrees due to thermal interface resistance and spurious radiative transfer. Thus, their experimental results do not represent the true D of the sample. Therefore, the D from these studies will not be compared and discussed thereafter. Although the thermocouple is in direct contact with the sample in our experiments, the compression at high pressure reduced the contact thermal resistance significantly. The diffused scattering of plagioclase exsolution was also absent in the recovered sample in our study. Based on our results, no radiative heat transfer occurred in our experiments at temperatures below 873 K.

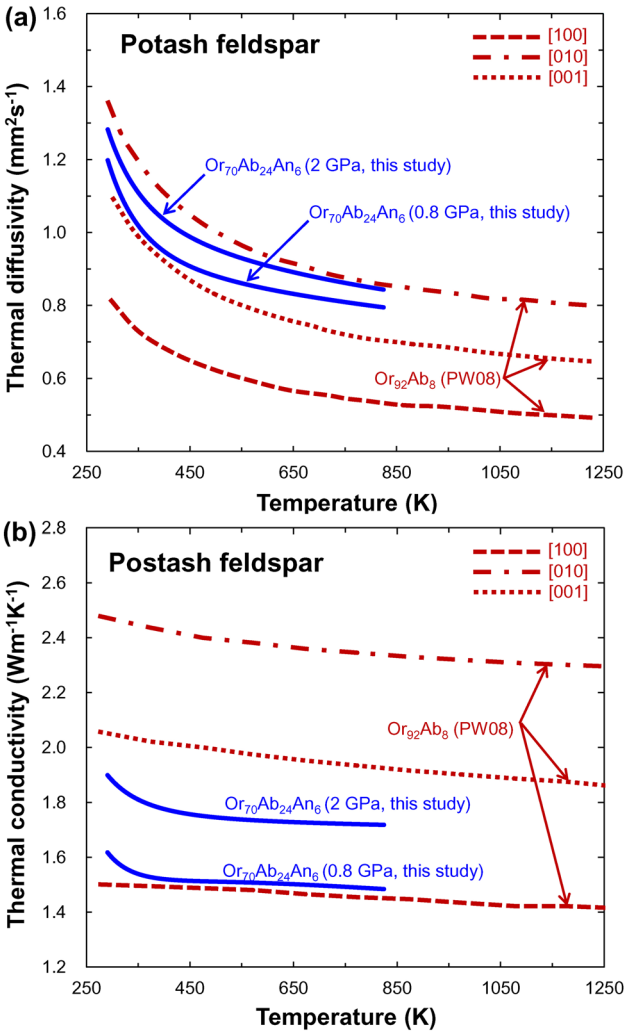

Fig. 7 Comparison of the D and κ of potash feldspar (**a**, **b**) with previous studies. Data sources: PW08 (Pertermann et al. 2008)

Figure 7b shows a comparison of κ of perthite from various studies. In most cases, the κ was indirectly calculated from the relation $\kappa = \rho D C_p$ rather than measured directly. As shown in Fig. 7b, the calculated κ of the single-crystal low sanidine ($Or_{92}Ab_8$) in three directions from the D reported by Pertermann et al. (2008) indicates a very weak temperature dependence. When temperature increased from 300 to 1250 K, a 9.5% decrease in calculated κ was observed. This trend is in agreement with the experimentally determined κ of perthite in this study. Figure 7b shows that the values of κ of perthite measured at 0.5 and 2 GPa lie between those of single-crystal low-sanidine along the [001] and [100] directions (Pertermann et al. 2008).

Figure 8a compares the D of Ab with various chemical components measured at high temperature. Linvill et al. (1984) first reported the D of polycrystalline Ab ($Ab_{99}An_1$) at ambient pressure and a narrow temperature range (273–450 K), in which D reduced quickly with the increase in temperature. Hofmeister et al. (2009) measured the D of a natural single-crystal Ab ($Ab_{98.2}Or_{1.6}$) as a function of temperature using the LFA. Their results indicated that at low temperature (< 650 K), the D in three directions rapidly decreased with the increase in temperature, whereas the D decreased slowly at high temperatures (> 700 K) (Fig. 8a). The values of D in three directions yielded $D_{[010]} > D_{[001]} > D_{[100]}$. As illustrated in Fig. 8a, the results determined by Hofmeister et al. (2009) are in general agreement with our experimental data but are higher than those of natural plagioclase with compositions of $Ab_{78}An_{19}$ and $Ab_{51}An_{47}$, as reported by Branlund and Hofmeister (2012), at 1 atm pressure. The difference between the work of Branlund and Hofmeister (2012) and other studies (Fig. 8a) may be mainly due to the difference in Ab chemical composition. Another possible explanation is that the presence of Ab twins and inclusions in natural samples used by Branlund and Hofmeister (2012) produced grain boundary interface resistance at low temperatures and thus reduced the heat transfer efficiency (Smith et al. 2003).

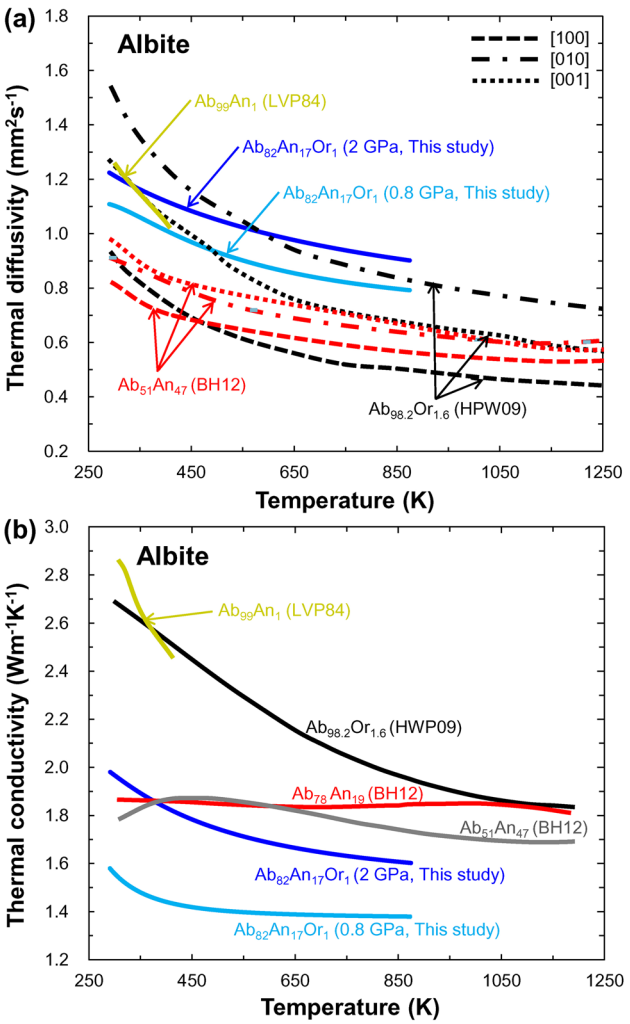

Fig. 8 Comparison of the D and κ of albite (**a**, **b**) with previous studies. Data sources: LVP84 (Linvill et al. 1984); PW08 (Pertermann et al. 2008); HWP09 (Hofmeister et al. 2009); BH12 (Branlund and Hofmeister 2012)

Figure 8b shows a comparison of the temperature dependence of κ of Ab measured in this study with previous data. Similar to perthite, the κ of Ab from previous studies was obtained through formulas ($\kappa = C_P D\rho$). Linvill et al. (1984) determined the κ of $Ab_{99}An_1$ in a narrow temperature range (273–450 K). Hofmeister et al. (2009) obtained the bulk κ of natural single-crystal Ab ($Ab_{98.2}Or_{1.6}$) by geometric averaging of values along three orientations. Their results showed a rapid drop across the temperature range investigated and were considerably higher than ours. This finding is mainly due to the lower Ab content of our samples ($Ab_{82}An_{17}Or_1$) compared with those in the work of Hofmeister et al. (2009). In addition, compared with the single-crystal sample, the polycrystalline Ab used in this study presented a further reduced κ, which is due to the presence of grain boundary interfacial resistance (Smith et al. 2003; Fu et al. 2019; Zhang et al. 2019a). Branlund and Hofmeister (2012) calculated the κ of several Abs ($Ab_{78}An_{19}$ and $Ab_{51}An_{47}$), and their temperature dependences were not evident. Their κ was consistent with the experimentally determined κ of Ab at 2 GPa in this study.

Heat capacity of perthite and Ab

We calculated the specific heat capacities of perthite and Ab at 1 atm and the pressure dependence of specific heat capacity at room temperature (Fig. 9). The calculated heat capacities at 1 atm based on this study were notably lower than previously measured ones (Or from the work of Akaogi et al. 2004; $Ab_{40}An_{60}$ from the work of Benisek et al. 2009), especially at high temperatures (Fig. 9a, b). The pressure dependence of specific heat capacity of perthite and Ab slightly increased with the increase in pressure (about 5% GPa^{-1}) (Fig. 9c, d, respectively). The largest differences between the calculated and measured specific heat capacity for perthite and Ab were 20% and 65% at 800 K, respectively. For synthetic polycrystalline olivine, the transient plane-source method has been shown to be a reliable method for deducing heat capacities, since the calculation (Zhang et al. 2019a, b) gives values highly consistent with direct measurements (Anderson and Isaak 1995). In the present study, the experimental technique adopted is the same as that used by Zhang et al. (2019a, b), whereas the starting materials used in this study extremely differed from those in heat capacity measurement (Akaogi et al. 2004; Benisek et al. 2009). Thus, the chemical composition, microstructure, and porosity may influence the heat capacity of silicate materials, which may cause the contradiction observed.

Effect of chemical composition on heat transfer properties

Figure 10a shows the effect of variable chemical composition on the D of feldspar (Linvill et al. 1984; Pertermann et al. 2008; Hofmeister et al. 2009; Branlund and Hofmeister 2012). The bulk D of the single-crystal sample (Ab_8Or_{92}, $Ab_{98.2}An_{0.2}Or_{1.6}$, $Ab_{78}An_{19}$, $Ab_{53}An_{47}$, and $Ab_{41}An_{59}$) (Höfer and Schilling 2002; Pertermann et al. 2008; Hofmeister et al. 2009; Branlund and Hofmeister 2012) was obtained by geometric averaging of D along three different directions. Our experimental results for D and κ at high temperature and pressure were extrapolated at 1 atm pressure using Eqs. (5–6). The D for most alkali feldspars was in the range of 0.8–1.26 mm^2s^{-1} at room temperature, whereas it decreased to a constant value of 0.6 ± 0.1 mm^2s^{-1} when the temperature exceeded 900 K. In particular, the D of Ab at room temperature was the highest, and that of An was the lowest compared with other endmembers of feldspar (Fig. 10a). As a result, the D for

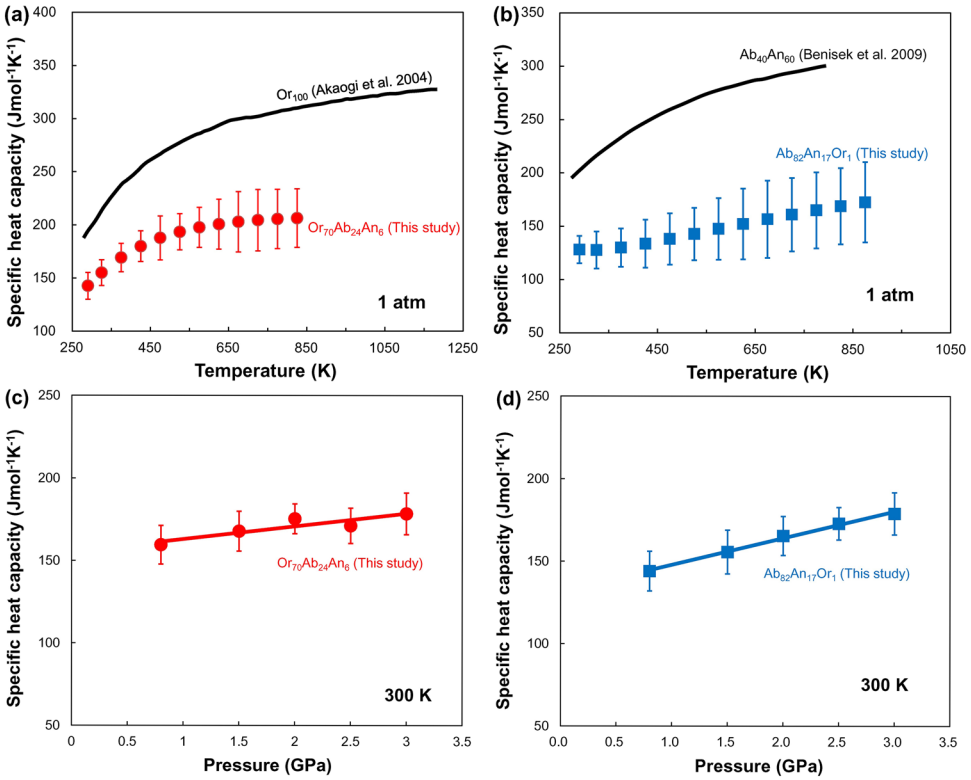

Fig. 9 Temperature dependence of heat capacity of **a** perthite and **b** albite at 1 atm. Pressure dependence of heat capacity of **c** perthite and **d** albite at room temperature. Black solid lines denote the reference $C_P(T)$ of orthoclase (Akaogi et al. 2004) and $Ab_{40}An_{60}$ (Benisek et al. 2009)

alkali feldspars systematically decreased with the decrease in Ab content and the increase An content. This could be due to Ab being well ordered at room temperature. However, the samples with intermediate compositions exhibited a reduced order because of the additional cations and therefore presented reduced *D*. In addition, has an ordered although An arragement, it has a large primitive cell with a number of atoms, which also reduced *D* (Hofmeister 2010; Branlund and Hofmeister 2012).

Figure 10b exhibits the effect of different compositions on the κ of feldspar at 1 atm pressure. The results show that the κ of different components at room temperature ranged from 1.3 to 2.86 $Wm^{-1}K^{-1}$, and the κ of samples with a high Ab content (> 98) was the highest among all experimental results. The κ of feldspar with high Ab content (> 98) showed a relatively strong temperature dependence (Linvill et al. 1984; Hofmeister et al. 2009) throughout the temperature range investigated, whereas an extremely weak temperature of κ was found in this study and for feldspars with a low Ab content (Pertermann et al. 2008; Branlund and Hofmeister 2012). The effect of chemical composition on the κ of binary solid solutions can be evaluated from their two end members (Padture and Klemens 1997; Marquardt et al. 2009; Wang et al. 2014; Ohta et al. 2017; Zhang et al. 2019b). Padture and Klemens (1997) proposed a model that predicts the effect of scattering by solute atoms on κ:

$$\kappa = \kappa_i \left(\frac{\omega_0}{\omega_M}\right) \arctan\left(\frac{\omega_M}{\omega_0}\right) \tag{7}$$

with

$$\left(\frac{\omega_0}{\omega_M}\right)^2 = \left(\frac{\chi T}{C(1-C)}\right) \tag{8}$$

where ω_M is the phonon frequency corresponding to the maximum of the acoustic branch of the phonon spectrum, ω_0 is the phonon frequency at which the intrinsic mean free path is equal to that due to solute atoms, χ is a constant, and C is the concentration of solute atoms. In the case of the $Ab_xOr_{(100-x)}$ system, κ_i is the thermal conductivity of solid solutions without the solute-atom phonon scattering and is given by the following:

$$\kappa_i = C\kappa_{Or} + (1-C)\kappa_{Ab} \tag{9}$$

where κ_{Ab} and κ_{Or} are the thermal conductivity of Ab and Or at given temperature from the literature, respectively (Pertermann et al. 2008; Branlund and Hofmeister 2012). As displayed in Fig. 11, the *D* and κ under 1 atm pressure can be fitted by Eqs. (7–9) at different temperatures, and the constant χ values approximated 3.51×10^{-4} and 1.37×10^{-4} K^{-1}, respectively. Nevertheless, the fitting results for *D* were better than those for κ. The minimum thermal conductivity was predicted to occur with the $Ab_{35}Or_{65}$ composition. The

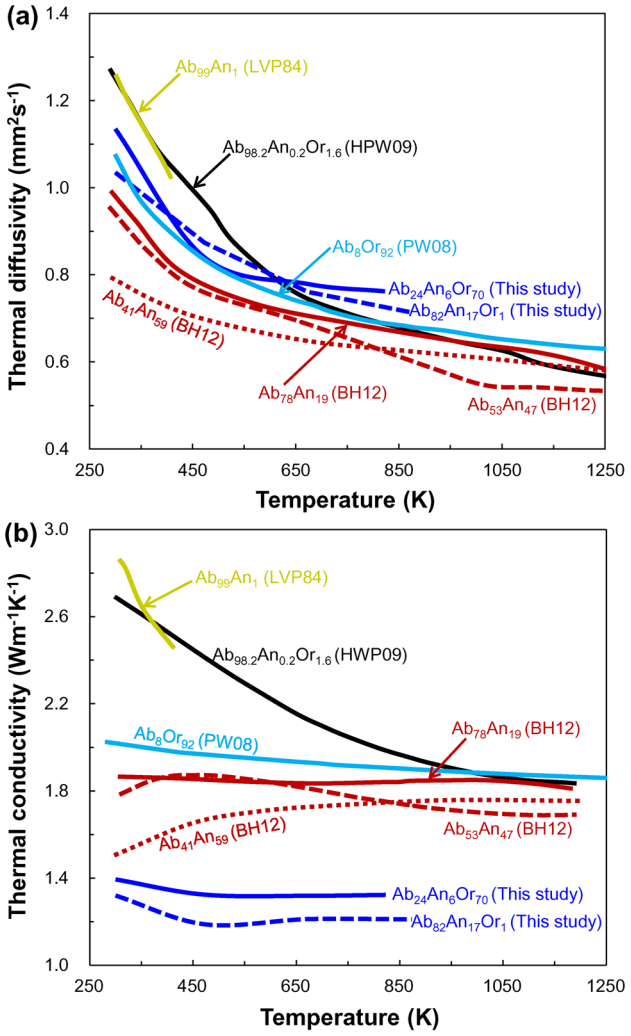

Fig. 10 Effect of chemical composition on D (**a**) and κ (**b**) of feldspars at 1 atm pressure. Data sources: LVP84 (Linvill et al. 1984); PW08 (Pertermann et al. 2008); HWP09 (Hofmeister et al. 2009); BH12 (Branlund and Hofmeister 2012)

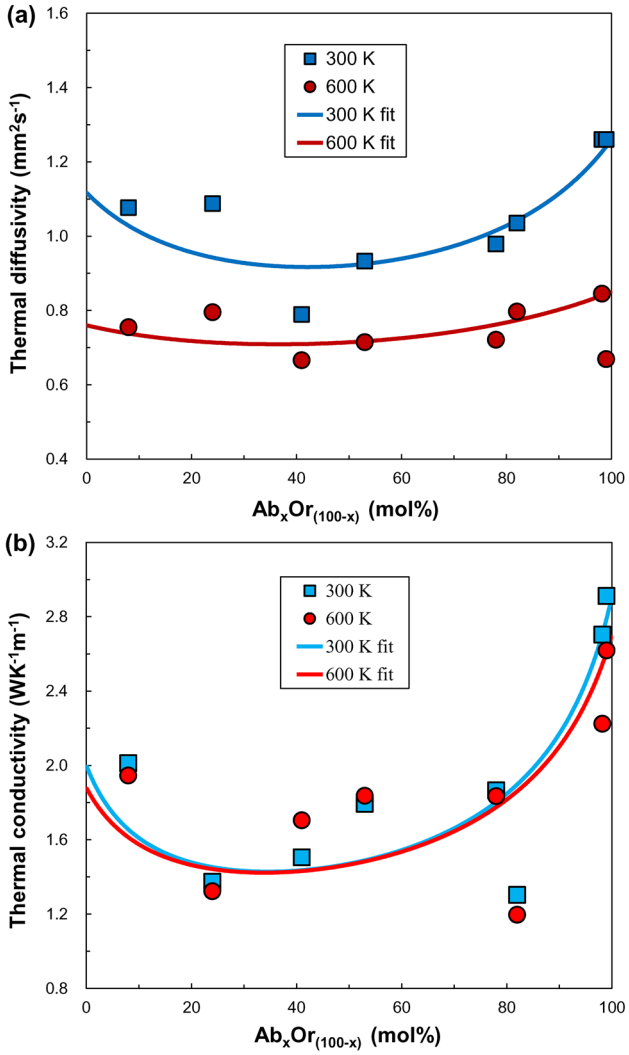

Fig. 11 D (**a**) and κ (**b**) of alkaline feldspar solid solution $Ab_xOr_{(1-x)}$ as a function of Ab content at 300 K and 600 K under 1 atm pressure. Data sources: LVP84 (Linvill et al. 1984); PW08 (Pertermann et al. 2008); HWP09 (Hofmeister et al. 2009); BH12 (Branlund and Hofmeister 2012)

significant effect of scattering by solute atoms on D and κ can be observed from the downward curves of the theoretical predictions. This finding is explained by the distortion of lattice near the solute atoms, which results in the disturbance of lattice vibrations. However, this influence gradually decreased with the increase in temperature.

Implications for the mean thermal conductivity of the crust and the thermal structure of the lithosphere

The thermal evolution of the planet's crust and lithosphere depends largely on the heat transfer rate (Rudnick et al. 1998; Petitjean et al. 2006; Whittington et al. 2009). In the crust, heat from deep Earth is mainly transmitted by conduction, except for fluid- or magma-rich environments where thermal convection dominates. The efficiency of heat transfer is mainly controlled by thermal conductivity of the Earth's crust. Thermal transport properties (D and κ) are among the most important parameters of rocks and minerals, and they can be used to model the thermal structure and dynamics of the deep Earth. The D and κ have a strong temperature and pressure dependence (Vosteen and Schellschmidt 2003; Mottaghy et al. 2008; Fu et al. 2019; Zhang et al. 2019a, b; Xiong and Zhang 2019; Ge et al. 2021). Given the lack of direct measurment of κ for minerals and rocks at high temperatures and pressures, previous thermal models assumed that the κ of the Earth's lithosphere is constant and is indirectly calculated from D, whereas the pressure dependence was not considered (Stein and Stein 1992;

McKenzie et al. 2005; Michaut et al. 2007; Whittington et al. 2009; Nabelek et al. 2012; Merriman et al. 2013; Lemenager et al. 2018). In this study, we recalculated the average κ of the Earth's crust based on the mineralogy model of 30% quartz, 60% Ab, 5% phlogopite, and 5% annite (Whittington et al. 2009), with consideration of the pressure effect on thermal properties. For κ of quartz, we use the polycrystalline data described in Gibert and Mainprice (2009), and the κ of Ab was obtained from our results. The κ of phlogopite and annite was obtained from the work of Hofmeister and Carpenter (2015), in which annite was replaced by biotite. Moreover, the geothermal gradient was assumed to be 15 Kkm^{-1}. The increase in density due to compression was partially offset by the decrease in density due to high temperature. This change was small compared with the changes in C_P and κ and is thus not considered here.

Figure 12 shows the average κ profile of the crust based on the above assumptions. The κ decreases with the increase in temperature (< 850 K), from 3.71 $Wm^{-1}K^{-1}$ at the Earth's surface to 1.73 $Wm^{-1}K^{-1}$ at the quartz phase transition (α–β) condition. At high temperatures (> 850 K), κ increased slightly because the κ of quartz (Gibert and Mainprice 2009) gradually increased with temperature. The κ of the lower crust (about 850 K) calculated from the present study is 10% lower than that estimated by Whittington et al. (2009) and 33% lower than that estimated by Chapman and Furlong (1992). Figure 12 shows that the κ of the lithospheric mantle inferred from the κ of olivine (Pertermann and Hofmeister 2006) is considerably higher than that of the lower crust.

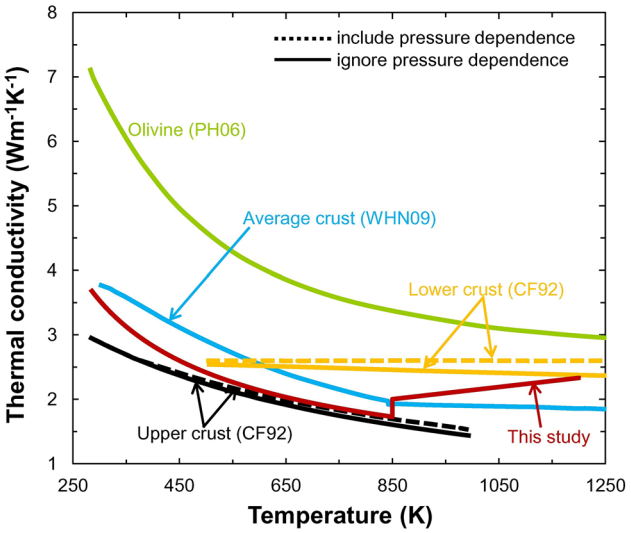

Fig. 12 Average crustal thermal conductivity as a function of temperature using a mineralogical model proposed by Whittington et al. (2009). The solid lines ignore pressure dependence and the dotted lines include pressure dependence. Data sources: CF92 (Chapman and Furlong 1992); PH06 (Pertermann and Hofmeister 2006); WHN09 (Whittington et al. 2009)

This observation suggests that the lower crust is a good thermal insulator and effectively prevents rapid heat loss from the Earth's interior through the lithosphere.

Temperature distribution in the lithosphere affects various physical properties and processes, such as rock melting, electrical and magnetic properties, and seismic properties (Chapman 1986). Therefore, the effect of variable κ of the crust on the lithospheric geothermal structure is discussed based on the κ curves of the crust from the work of Whittington et al. (2009) and this study. We assumed that heat in the lithosphere is mainly transferred by heat conduction based on one-dimension steady-state conductive geotherms (Chapman 1986; Furlong and Chapman 2013; Miao et al. 2014). The finite element method was applied to solve the Fourier heat conduction in one dimension as follows (Chapman 1986; Furlong and Chapman 2013):

$$\rho C_p \frac{\partial T}{\partial t} = \frac{\partial}{\partial x} k(T,P) \frac{\partial T}{\partial x} + H \tag{10}$$

where C_P is the heat capacity, T is the temperature in K, t is the time in years, H is the radiative heat production, and x is the depth in m. To simplify the model, we calculated the depth from the upper crust to the deeper part of the lithosphere with a 10 m step size and considered heat conduction as the only mechanism of heat transfer. The density was assumed to be constant at 2700 kgm^{-3} (Whittington et al. 2009). In our calculation, the crust is divided into an upper crust of 16 km thickness and a lower crust of 23 km thickness. The pressure and temperature dependences of κ and C_P from feldspar samples were applied. Based on previous heat generation data (Hasterok and Chapman 2011), we adopted radiative heat production values of 1, 0.4, and 0.02 $\mu W\ m^{-3}$ for the upper crust, lower crust, and upper mantle, respectively. In addition, three different reference surface heat fluxs of 50, 70, and 90 $mW\ m^{-2}$ were used. The mantle adiabat was referenced from the work of Thompson (1992), and the surface temperature was fixed to 283 K.

Figure 13 illustrates the calculated temperature profiles in the lithosphere from two thermal conductivity models. When the surface heat flows were 50, 70, and 90 mWm^{-2}, the mean thermal thicknesses of lithosphere were 150, 68, and 39 km from our estimations, respectively; the values were 127, 58, and 40 km according to Whittington et al. (2009). Notably, the pressure dependence of κ was considered in this calculation, whereas such pressure effect was disregarded in the calculations by Whittington et al. (2009). These observations suggest that pressure plays an important role in the estimation of the mean thermal thicknesses of the lithosphere. At the depth of 21 km (Fig. 13), the temperature estimated from our geothermal gradient model was higher by 216 K than that estimated by Whittington et al. (2009) at the same heat flow of 90 mWm^{-2}. This difference will cause a great uncertainty in the estimation of melting

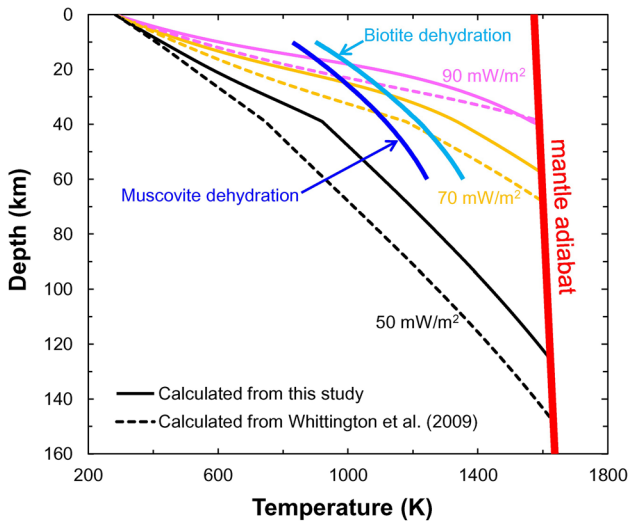

Fig. 13 Effects of different crustal thermal conductivity curves on lithospheric geotherms. Surface heat flow: 50 mWm^{-2}, 70 $mW\ m^{-2}$, 90 mWm^{-2}. Solid black line: mantle adiabatic line ($T_m = 1573 + 0.4 \times Z$, Z is depth); solid lines: geotherms calculated from the present data; dashed lines: geotherms calculated from Whittington et al (2009). Solidus curves of muscovite and biotite dehydration (Patiño Douce and Harris 1998) are also shown

temperature in regions with high heat flux such as southern Tibet. Figure 13 shows a comparison of our calculated geotherms with the solidus curves of muscovite and biotite dehydration (Patiño Douce and Harris 1998). Evidently, our estimated temperature profile suggestes that partial melting will occur at shallow depths of the middle and lower crust, consistent with the depth of partial melting derived from the κ of granitoids (Fu et al. 2019). Thus, the present estimate may provide a new understanding of the low-velocity and high-conductivity anomalies observed in the crust (Nelson et al. 1996; Wei et al. 2001; Li et al. 2003; Hacker et al. 2014; Zhang et al. 2021).

Conclusions

The D and κ of two natural alkali feldspars were investigated as a function of temperature (300–873 K) and pressure (up to 3 GPa) using the transient plane-source method. The present experimental data show that the D and κ of two alkali feldspar samples decreased with the increase in temperature and increased linearly with pressure, whereas the κ of perthite remained unchanged when the temperature was higher than 450 K. The D for alkali feldspars systematically decreased with the decrease in Ab content and the increase in An content. The κ of feldspar with a high Ab content showed a relatively strong temperature dependence throughout the temperature range investigated, whereas a very weak temperature of κ was found for feldspar with a lower Ab content. By combining the measured thermal properties and surface flows, the present calculated geotherms suggest that the thermal thickness of the lithosphere is thick for regions with low heat flow and thin for regions with high heat flow. Moreover, a comparison of the solidus curves of muscovite and biotite dehydration with the calculated temperature profiles implies that partial melting will occur at shallow depths of the crust, which provides additional constraints on the partial melting model to explain the low-velocity and high-conductivity anomalies observed in the crust.

Supplementary Information The online version contains supplementary material available at https://doi.org/10.1007/s00410-021-01797-2.

Acknowledgements We thank the editor (H. Keppler) and two anonymous reviewers for their constructive comments that greatly improved the manuscript. This study was supported by Key Research Program of Frontier Sciences of CAS (ZDBS-LY-DQC015), CAS "Light of West China" program (Y9CR026 to X. G.), NSF of China (41773056, 41973056, 42072051). The authors declare no competing financial interests.

References

Akaogi M, Kamii N, Kishi A, Kojitani H (2004) Calorimetric study on high-pressure transitions in $KAlSi_3O_8$. Phys Chem Mineral 31:85–91

Anderson OL (1999) Mantle convection: a thermal balancing act. Science 283:1652–1653

Anderson OL, Isaak DG (1995) Elastic constants of mantle minerals at high temperature. Mineral Phys Crystallogr Handb Phys Constants 2:64–97

Benisek A, Dachs E, Kroll H (2009) Excess heat capacity and entropy of mixing in high structural state plagioclase. Am Mineral 94:1153–1161

Benusa MD, Angel RJ, Ross NL (2005) Compression of albite, $NaAlSi_3O_8$. Am Mineral 90:1115–1120

Branlund JM, Hofmeister AM (2012) Heat transfer in plagioclase feldspars. Am Mineral 97:1145–1154

Chapman DS (1986) Thermal gradients in the continental crust. Geol Soc Lond Spec Publ 24:63–70

Chapman DS, Furlong KP (1992) Thermal state of the continental crust. In: Fountain DM, Arculus R, Kay RW (eds) Continental lower crust. Elsevier, Amsterdam, pp 179–199

Dzhavadov LN (1975) Measurement of thermophysical properties of dielectrics under pressure. High Temp High Press 7:49–54

Fu HF, Zhang BH, Ge JH, Xiong ZL, Zhai SM, Shan SM, Li HP (2019) Thermal diffusivity and thermal conductivity of granitoids at 283–988 K and 0.3–1.5 GPa. Am Mineral 104:1533–1545

Furlong KP, Chapman DS (2013) Heat flow, heat generation, and the thermal state of the lithosphere. Annu Rev Earth Planet Sci 41:385–410

Ge JH, Zhang BH, Xiong ZL, He LF, Li HP (2021) Thermal properties of harzburgite and dunite at 0.8–3 GPa and 300–823 K and implications for the thermal evolution of Tibet. Geosci Front 12:947–956

Gibert B, Mainprice D (2009) Effect of crystal preferred orientations on the thermal diffusivity of quartz polycrystalline aggregates at high temperature. Tectonophysics 465:150–163

Hacker BR, Ritzwoller MH, Xie J (2014) Partially melted, mica-bearing crust in Central Tibet. Tectonics 33:1408–1424
Hasterok D, Chapman DS (2011) Heat production and geotherms for the continental lithosphere. Earth Planet Sci Lett 307:59–70
Höfer M, Schilling FR (2002) Heat transfer in quartz, orthoclase, and sanidine at elevated temperature. Phys Chem Mineral 29:571–584
Hofmeister AM (1999) Mantle values of thermal conductivity and the geotherm from phonon lifetimes. Science 283:1699–1706
Hofmeister AM (2007) Pressure dependence of thermal transport properties. Proc Natl Acad Sci USA 104:9192–9197
Hofmeister AM (2010) Thermal diffusivity of oxide perovskite compounds at elevated temperature. J Appl Phys 107:103532
Hofmeister AM, Branlund JM, Pertermann M (2007) Properties of rocks and minerals–thermal conductivity of the earth. Treatise Geophys 2:543–577
Hofmeister AM, Whittington AG, Pertermann M (2009) Transport properties of high albite crystals, near-endmember feldspar and pyroxene glasses, and their melts to high temperature. Contrib Mineral Petrol 158:381–400
Hofmeister AM, Dong J, Branlund JM (2014) Thermal diffusivity of electrical insulators at high temperatures: Evidence for diffusion of bulk phonon-polaritons at infrared frequencies augmenting phonon heat conduction. J Appl Phys 115:163517
Hofmeister AM, Carpenter PK (2015) Heat transport of micas. Can Mineral 53:557–570
Kanamori H, Fujii N, Mizutani H (1968) Thermal diffusivity measurement of rock-forming minerals from 300 to 1100 K. J Geophys Res 73:595–605
Lemenager A, O'Neill C, Zhang S, Evans M (2018) The effect of temperature-dependent thermal conductivity on the geothermal structure of the sydney basin. Geotherm Energy 6:1–27
Li S, Unsworth MJ, Booker JR, Wei W, Tan H, Jones AG (2003) Partial melt or aqueous fluid in the mid-crust of Southern Tibet? Constraints from INDEPTH magnetotelluric data. Geophys J Int 153:289–304
Linvill ML, Vandersande JW, Pohl RO (1984) Thermal conductivity of feldspars. Bull Mineral 107:521–527
Marquardt H, Ganschow S, Schilling FR (2009) Thermal diffusivity of natural and synthetic garnet solid solution series. Phys Chem Mineral 36:107–118
McKenzie D, Jackson J, Priestley K (2005) Thermal structure of oceanic and continental lithosphere. Earth Planet Sci Lett 233:337–349
Merriman JD, Whittington AG, Hofmeister AM, Nabelek PI, Benn K (2013) Thermal transport properties of major archean rock typesto high temperature and implications for cratonic geotherms. Precambrian Res 233:358–372
Miao S, Li H, Chen G (2014) The temperature dependence of thermal conductivity for lherzolites from the North China Craton and the associated constraints on the thermodynamic thickness of the lithosphere. Geophys J Inter 197:900–909
Michaut C, Jaupart C, Bell DR (2007) Transient geotherms in Archean continental lithosphere: new constraints on thickness and heat production of the subcontinental lithospheric mantle. J Geophys Res 112:1–17
Mottaghy D, Vosteen HD, Schellschmidt R (2008) Temperature dependence of the relationship of thermal diffusivity versus thermal conductivity for crystalline rocks. Int J Earth Sci 97:435–442
Nabelek PI, Hofmeister AM, Whittington AG (2012) The influence of temperature-dependent thermal diffusivity on the conductive cooling rates of plutons and temperature-time paths in contact aureoles. Earth Planet Sci Lett 317:157–164
Nelson KD, Zhao W, Brown LD, Kuo J, Che J, Liu X, Klemperer SL, Makovsky Y, Meissner R, Mechie J, Kind R, Wenzel F, Ni J, Nabelek J, Leshou C, Tan H, Wei W, Jones AG, Booker J, Unsworth M, Kidd W, Hauck M, Alsdorf D, Ross A, Cogan M, Wu C, Sandvol W, Edwards M (1996) Partially molten middle crust beneath southern Tibet: synthesis of project INDEPTH results. Science 274:1684–1688
Nestola F, Curetti N, Benna P, Ivaldi G, Angel RJ, Bruno E (2008) Compressibility and high-pressure behavior of $Ab_{63}Or_{27}An_{10}$ anorthoclase. Can Mineral 46:1443–1454
Ohta K, Yagi T, Hirose K, Ohishi Y (2017) Thermal conductivity of ferropericlase in the Earth's lower mantle. Earth Planet Sci Lett 465:29–37
Osako M, Ito E, Yoneda A (2004) Simultaneous measurements of thermal conductivity and thermal diffusivity for garnet and olivine under high pressure. Phys Earth Planet Inter 143:311–320
Osako M, Yoneda A, Ito E (2010) Thermal diffusivity, thermal conductivity, and heat capacity of serpentine (antigorite) under high pressure. Phys Earth Planet Inter 183:229–233
Padture NP, Klemens PG (1997) Low thermal conductivity in garnets. J Am Ceram Soc 80:1018–1020
Patiño Douce AE, Harris N (1998) Experimental constraints on Himalayan anatexis. J Petrol 39:689–710
Pertermann M, Hofmeister AM (2006) Thermal diffusivity of olivine-group minerals at high temperature. Am Mineral 91:1747–1760
Pertermann M, Whittington AG, Hofmeister AM, Spera FJ, Zayak J (2008) Transport properties of low-sanidine single-crystals, glasses and melts at high temperature. Contrib Mineral Petrol 155:689–702
Petitjean S, Rabinowicz M, Grégoire M, Chevrot S (2006) Differences between Archean and Proterozoic lithospheres: assessment of the possible major role of thermal conductivity. Geochem Geophys Geosyst 7:1–26
Rudnick RL, McDonough WF, O'Connell RJ (1998) Thermal structure, thickness and composition of continental lithosphere. Chem Geol 145:395–411
Smith JV, Brown WL (1988) Feldspar minerals: I crystal structures, physical, chemical and microtextural properties, 2nd edn. Springer, Berlin, pp 1–20
Smith DS, Fayette S, Grandjean S, Martin C, Telle R, Tonnessen T (2003) Thermal resistance of grain boundaries in alumina ceramics and refractories. J Am Ceram Soc 86:105–111
Stein CA, Stein SA (1992) A model for the global variation in oceanic depth and heat flow with lithospheric age. Nature 359:123–129
Thompson AB (1992) Water in the Earth's upper mantle. Nature 358:295–302
Vosteen HD, Schellschmidt R (2003) Influence of temperature on thermal conductivity, thermal capacity and thermal diffusivity for different types of rock. Phys Chem Earth 28:499–509
Wang C, Yoneda A, Osako M, Ito E, Yoshino T, Jin Z (2014) Measurement of thermal conductivity of omphacite, jadeite, and diopside up to 14 GPa and 1000 K: Implication for the role of eclogite in subduction slab. J Geophys Res Solid Earth 119:6277–6287
Wei W, Unsworth M, Jones A, Booker J, Tan H, Nelson D, Chen L, Li S, Solon K, Bedrosian P, Jin S, Deng M, Ledo J, Kay D, Robert B (2001) Detection of widespread fluids in the Tibetan crust by magnetotelluric studies. Science 292:716–718
Whittington AG, Hofmeister AM, Nabelek PI (2009) Temperature-dependent thermal diffusivity of the Earth's crust and implications for magmatism. Nature 458:319–321
Xiong ZL, Zhang BH (2019) Thermal properties of olivine, wadsleyite and ringwoodite—a review. Minerals 9:519
Yanagawa TKB, Nakada M, Yuen DA (2005) Influence of lattice thermal conductivity on thermal convection with strongly temperature-dependent viscosity. Earth Planet Space 57:15–28

Zhang BH, Ge JH, Xiong ZL, Zhai SM (2019a) Effect of water on the thermal properties of olivine with implications for lunar internal temperature. J Geophys Res Planet 124:3469–3481

Zhang Y, Yoshino T, Yoneda A, Osako M (2019b) Effect of iron content on thermal conductivity of olivine with implications for cooling history of rocky planets. Earth Planet Sci Lett 519:109–119

Zhang BH, Guo X, Yoshino T, Xia QK (2021) Electrical conductivity of melts: Implications for conductivity anomalies in the Earth's mantle. Natl Sci Rev 8:nwab064. https://doi.org/10.1093/nsr/nwab064

Zheng YF, Chen YX (2016) Continental versus oceanic subduction zones. Natl Sci Rev 3:495–519